frontiers | Frontiers in Earth Science

TYPE Original Research
PUBLISHED 09 July 2024
DOI 10.3389/feart.2024.1427994

OPEN ACCESS

EDITED BY
Wenbin Tang,
Chengdu University of Technology, China

REVIEWED BY
Xiucheng Tan,
Southwest Petroleum University, China
Oumar Ibrahima Kane,
Chengdu University of Technology, China
Michelle Tiong,
Curtin University, Australia

*CORRESPONDENCE
Jianqin Xue,
XueJQ_petrochina@163.com

RECEIVED 05 May 2024
ACCEPTED 14 June 2024
PUBLISHED 09 July 2024

CITATION
Liu G, Xue J, Wu K, Wu S, Zhang B, Liu Z and Xing H (2024), Paleogene-Neogene ring-shaped sedimentary system and reservoir characteristics in the Western depression of the Qaidam Basin.
Front. Earth Sci. 12:1427994.
doi: 10.3389/feart.2024.1427994

Paleogene-Neogene ring-shaped sedimentary system and reservoir characteristics in the Western depression of the Qaidam Basin

Guoyong Liu[1,2], Jianqin Xue[1,2]*, Kunyu Wu[1,2], Songtao Wu[3], Boce Zhang[1,2], Zhanguo Liu[3] and Haoting Xing[1,2]

[1]Qinghai Provincial Key Laboratory of Plateau Saline-Lacustrine Basinal Oil & Gas Geology, Dunhuang, China, [2]Qinghai Oilfield Company, PetroChina, Dunhuang, China, [3]PetroChina Research Institute of Petroleum Exploration and Development, Beijing, China

The Paleogene-Neogene strata in the Western Depression of the Qaidam Basin represent a primary focus for oil and gas exploration and development. Influenced by both terrigenous clastic influx and endogenic carbonate deposition, these strata exhibit significant variation in sedimentary systems and reservoir characteristics. This study comprehensively examines the depositional patterns and reservoir properties of the Paleogene-Neogene sequence across the inner, middle, and outer belts of the basin, employing core analysis, thin section petrography, and physical property assessment of reservoirs. Key findings include 1) The development of a concentric sedimentary system in the Western Depression during the Paleogene-Neogene period, characterized by increased carbonate mineral content and decreased clastic material from the periphery to the center of the basin. 2) Varied sedimentary facies associations across different zones, with the outer belt dominated by fan delta and braided river delta deposits, and the middle and inner belts characterized by near-shore shallow lacustrine carbonates and algal mat deposits, and offshore semi-to deep-lacustrine fine sediments, respectively. 3) The outer belt exhibits reservoirs with favorable physical properties and connectivity, while the inner and middle belts show high heterogeneity, indicating potential for lithological traps and shale oil exploration. These insights offer scientific guidance for further investigation into the depositional systems of lacustrine basins in the Western Depression of the Qaidam Basin and for identifying promising reservoirs.

KEYWORDS

ring-shaped, Qaidam Basin, sedimentary system, lacustrine basin filling, favorable facies zone

1 Introduction

The Qaidam Basin, situated at a high altitude on the northeastern Tibetan Plateau, is distinguished by its substantial petroleum and natural gas reserves (Bailey and Anderson, 1982; Guo et al., 2017a). This endorheic basin has garnered considerable attention through comprehensive geological and geophysical research efforts, which aim to elucidate the intricate processes underlying its formation and evolution (Hanson et al., 2001). Such

research, particularly on lacustrine sedimentary patterns, is pivotal for refining oil and gas exploration and development strategies in the basin (Fang et al., 2016; Yang et al., 2020; Liu et al., 2021).

An analysis of the existing body of research on the Qaidam Basin, perched at a high altitude on the northeastern Tibetan Plateau, indicates a significant focus on its discrete depressions (Metivier et al., 1998; Karplus et al., 2011). These investigations shed light on the localized sedimentary processes, depositional environments, and hydrocarbon potential, contributing to a nuanced understanding of this crucial oil exploration and development zone. Specifically, the western depression of the basin features a distinctive sedimentary system, influenced by a variety of physical, chemical, and biological processes, predominantly showcasing a saline lacustrine environment driven by terrigenous clastic contributions and endogenic carbonate formation (Li, 2004; Guo et al., 2019). The hydrologically closed lakes and playas in the western depression of the Qaidam Basin develop high-quality source rocks (Lowenstein et al., 1989; Phillips et al., 1993; Vengosh et al., 1995). Detailed seismic data and heavy mineral analyses have delineated a sedimentary structure of alluvial fans, deltas, and shallow lacustrine prevalent in the Paleogene of the Qigequan-Hongliuquan-Gasi area (Schubel and Lowenstein, 1997; Owen et al., 2006; Zhao, 2006), while petrological, grain size and core data from the Kunbei region highlight a retrogradational delta system (Tan et al., 2016; Liu et al., 2018). Recent exploratory efforts in the Zhahaquan, Youquanzi, and Kaitemilike areas have uncovered various tight reservoir types in the lacustrine facies, attributed to Paleogene terrestrial material supply variations (Rieser et al., 2006; Bush et al., 2016; Wei et al., 2019). The Yingxi and Ganchaigou area, influenced by ancient landforms, harbor large-scale reservoirs of semi-deep lacustrine shale and near-shallow lacustrine algal limestone (Zhu et al., 2022; Li et al., 2023a), underpinning a shale oil accumulation model characterized by source-reservoir integration and large-scale distribution, alongside a lateral accumulation model emphasizing vertical communication and multi-layer system enrichment (Shi et al., 2020). The Neogene period, marked by global cooling, the retreat of the Paratethys Sea, and multi-stage tectonic movement, saw a reduction in the basin and lacustrine basin extent due to diminished water vapor, favoring a fan and braided river deltas, and shallow lacustrine sedimentary system in the Western Depression of the Qaidam Basin (Sun et al., 2020; Zheng et al., 2023). This era's depositional patterns, particularly in the southwestern regions, exhibit an oblique distribution of beach and bar sand bodies (Wang et al., 2023). While in the northwest region of Dafengshan, Nanyishan, and Xiaoliangshan, multiple algal limestone sets extend from the lacustrine basin edge to shallow lacustrine areas (Wang et al., 2020). Despite the wealth of detail provided by these studies, a comprehensive synthesis integrating these insights into a unified model of the basin's sedimentary patterns is lacking (Li et al., 2022). This fragmented approach constrains our understanding of basin-wide processes and the interconnection between various depositional systems, a challenge compounded by the basin's vastness and geological diversity (Li et al., 2022). Moreover, the existing study often inadequately clarifies the relationship between source rocks and high-quality reservoirs (Wang et al., 2020; He et al., 2021), obstructing lithologic trap identification and complicating the optimization of oil and gas exploration and development on a large scale.

Through meticulous core observation and analysis, alongside thin section petrography and comprehensive evaluation of reservoir characteristics, this study methodically investigates the Paleogene-Neogene depositional patterns within the Western Depression of the Qaidam Basin. It introduces and delineates the concept of a "ring-shaped" sedimentary model, and scrutinizes reservoir attributes across various depositional belts. The outcomes of this research aim to offer robust scientific insights for enhancing oil and gas exploration efforts in the Western Depression.

2 Geologic setting and stratigraphy

The Qaidam Basin, a vast inland intermountain basin on the northern Tibetan Plateau, is delineated by the Altun strike-slip fault to the west, the Qilian thrust fault belt to the north, and the East Kunlun mountain strike-slip belt to the south (Arnaud et al., 2003; Cowgill et al., 2003; Xia et al., 2021; Tang et al., 2021a). Its Cenozoic evolution is linked to convergent tectonic forces along the plateau's northern margin, a process intimately connected with the Indo-Asian collision that prompted ongoing uplift, thickening, shortening, and lateral compression of the Tibetan Plateau (Tapponnier et al., 2001; Dupont-Nivet et al., 2002; Bao et al., 2017; Zhang et al., 2018a; Sun et al., 2019; Jian et al., 2023). This tectonic activity fostered the development of NW-SE-oriented thrust fold belts along the basin's edges (Cheng et al., 2021). Structural analysis reveals the basin's division into three major tectonic units: the Western Depression, the Sanhu Depression, and a fault block belt along the basin's northern edge (Figure 1; Guo et al., 2017b). In Qaidam Basin, the climate also controls sedimentation and erosion, forming a potential Martian environmental analogue (Pullen et al., 2011; Heermance et al., 2013; Rohrmann et al., 2013; Angles and Li, 2017). The Western Depression, lying near the Kunlun and Altun Mountains, emerged during the Paleogene-Neogene under compressional forces. This depression houses a sedimentary sequence of Paleogene-Neogene strata, accumulating to a depth of approximately 6–7 km, and primarily consists of terrestrial to lacustrine deposits, spanning follow stratigraphic layers (Lu et al., 2019; Li et al., 2022; Zhang et al., 2020): 1) Lulehe Formation (~56–~42.8 Ma) consists of siltstone and sandstone, 2) Lower Member of Xianganchaigou Formation (~42.8–~38 Ma) consists of dolomitic mudstone and siltstone, 3) Upper Member of Xianganchaigou Formation (~38–~22 Ma) consists of limestone, argillaceous limestone, gypsum bearing mudstone and salt, 4) Shangganchaigou Formation (~22–~14.9 Ma) consists of limestone, argillaceous limestone and algal limestone, 5) Xiayoushashan Formation (~14.9–~8.2 Ma) consists of mudstone, siltstone and sandstone (Figure 2). These formations comprise primarily fine-grained lacustrine deposits, dividing into five short cycles, and are noted for their hydrocarbon potential (Guo et al., 2019; Guo et al., 2020; Liu et al., 2021).

3 Materials and methods

This study utilizes a comprehensive exploration dataset provided by Qinghai Oilfield, China National Petroleum

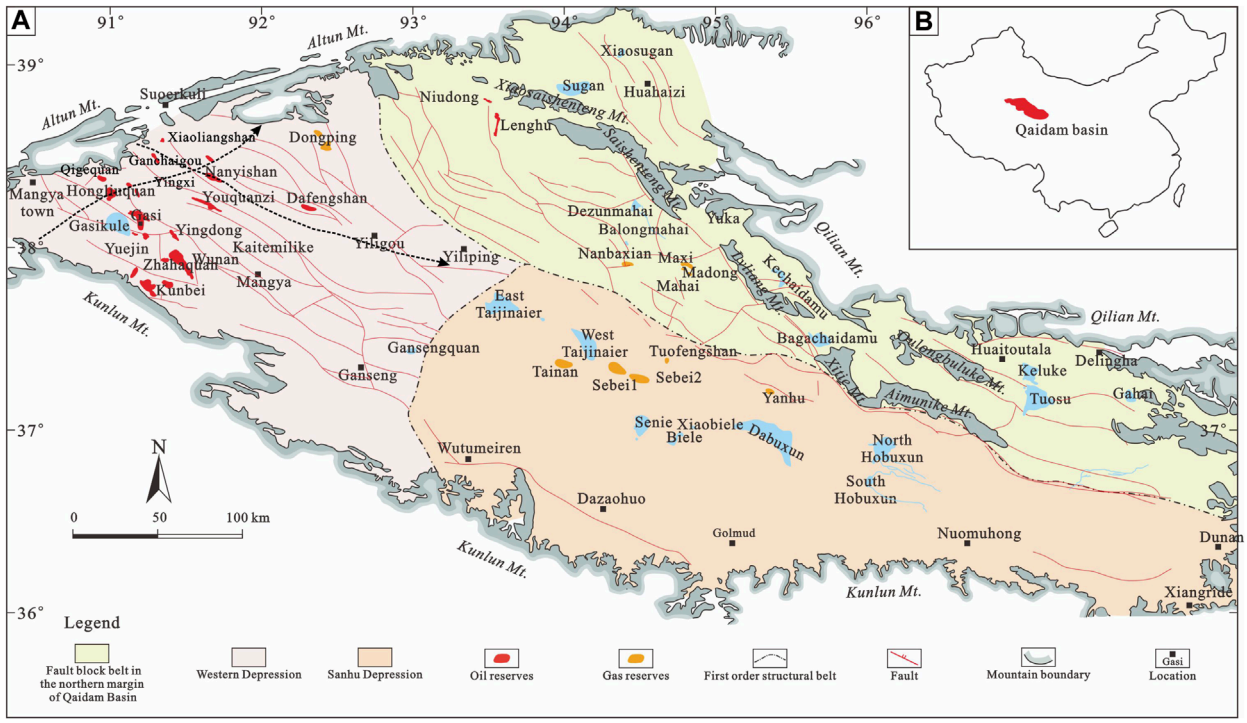

FIGURE 1
(A) Structural unit division map of Qaidam Basin (Modified from Tang et al., 2021a). The pink area delineates the Western Depression, which is the basin's primary region for oil and gas production, consisting predominantly of Cenozoic strata. The cyan area marks the northern margin fault block belt of the Qaidam Basin, recognized as the main region for Mesozoic gas production. The flesh-colored area represents the basin's Quaternary biogenic gas production zone. The two lines with arrows show the approximate locations of the two cross-well sections (NW-SE and SW-NE). **(B)** The diagram in the up right corner depicts the geographical location of the Qaidam Basin.

Corporation, comprising drill cores and wire-line logs. From this dataset, 20 representative well cross-sections across the Western Depression were compiled, based on over 100 wire-line logs. Detailed observations and descriptions were performed on 40 drill cores, exceeding a cumulative length of 1,000 m, that penetrated the Paleogene-Neogene strata within the Western Depression of the Qaidam Basin. These analyses were augmented by sedimentary structure and gamma-ray logs, calibrated at the cored wells, to conduct detailed sedimentary facies analysis for individual wells (Tang et al., 2021b; Kane et al., 2023). For the analysis, two typical cross sections were selected, one transverse and one parallel to the tectonic units (Figure 1).

Analysis of sedimentary facies offers an in-depth understanding of the sedimentary infill processes from the Paleogene to Neogene periods and the spatial distribution of various facies zones. This study examines the petrology, pore structure types, and physical properties of reservoirs across different facies zones to elucidate the temporal and spatial distribution of high-potential reservoirs. The relevant experiments were completed at Qinghai Provincial Key Laboratory of Plateau Saline-Lacustrine Basinal Oil & Gas Geology, with the ultimate aim of forming a sedimentation-reservoir exploration theory in the study area and laying the foundation for guiding oil and gas exploration in the Western depression of the Qaidam Basin.

4 Results

4.1 Sedimentary facies analysis

Based on comprehensive core observations and descriptions, various lithofacies have been classified. This classification, in conjunction with gamma-ray (GR) log characteristics, facilitates a facies association analysis. Within the study area, the lithofacies are categorized into braided river delta, near-shore shallow lacustrine, and offshore semi-deep to deep lacustrine facies.

4.1.1 Braided river delta and/or fan delta

The facies association of the braided river and/or fan delta plain is not present, and the distinction between pre-delta and lacustrine facies is challenging. Conversely, the braided river and/or fan delta front facies association is marked by the presence of low-angle cross-bedding in cores and a directional arrangement of gravel, indicative of bottomset deposits. Suspended gravels are occasionally visible at the base of relatively coarse-grained sandstone. The gamma-ray (GR) log exhibits box-type signatures and a positive grain sequence, both suggestive of sedimentary processes within subaqueous distributary channels (Figure 3A). Siltstone and argillaceous siltstone fill between these channels, where mouth bars are absent.

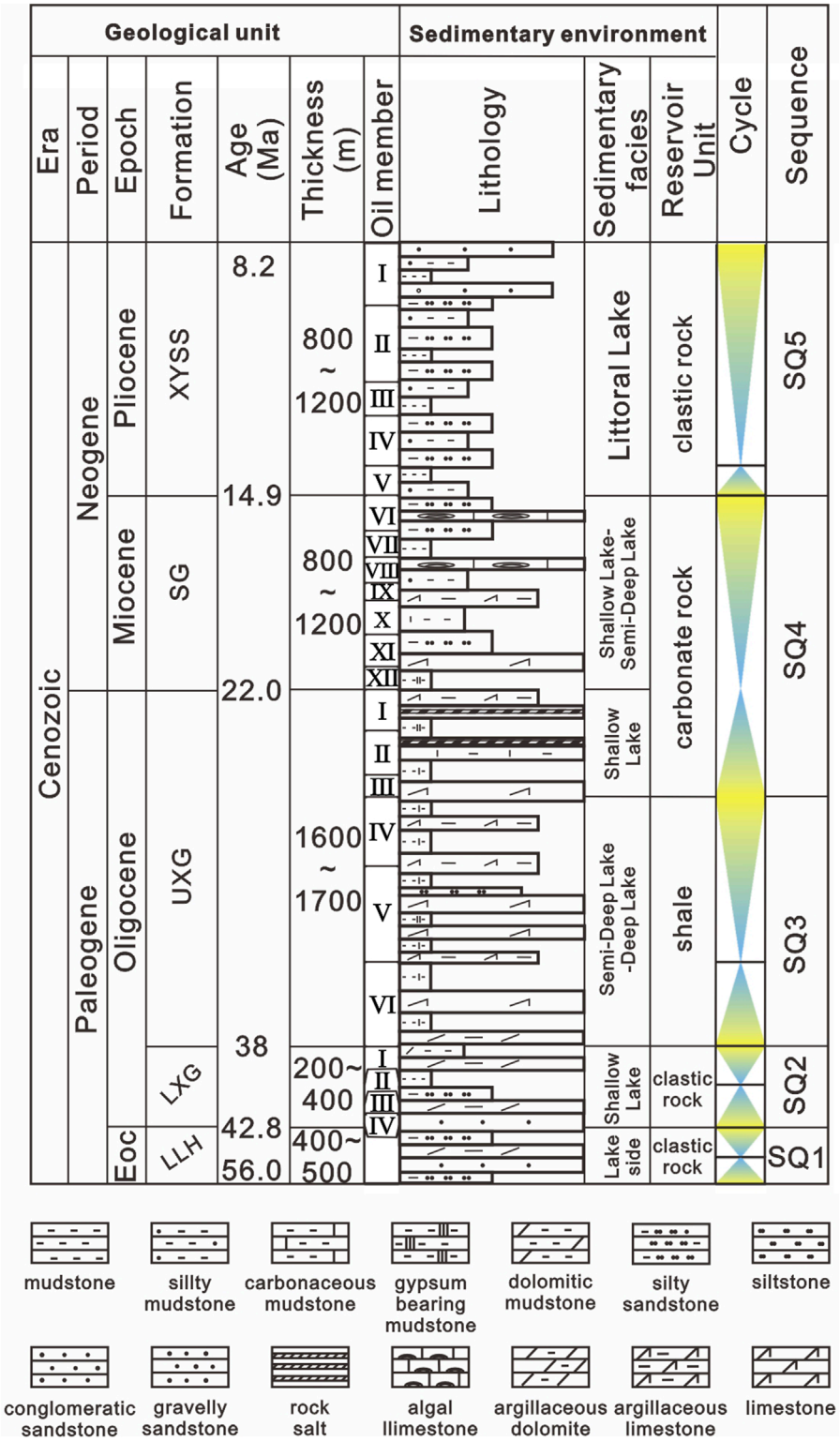

FIGURE 2
Stratigraphic column map of the Western Depression (Modified from Li et al., 2022). The abbreviations are used for stratigraphy in the figure, as follows: Lulehe Formation (LLH), Lower Member of Xiaganchaigou Formation (LXG), Upper Member of Xiaganchaigou Formation (UXG), Shangganchaigou Formation (SG), Xiayoushashan Formation (XYSS).

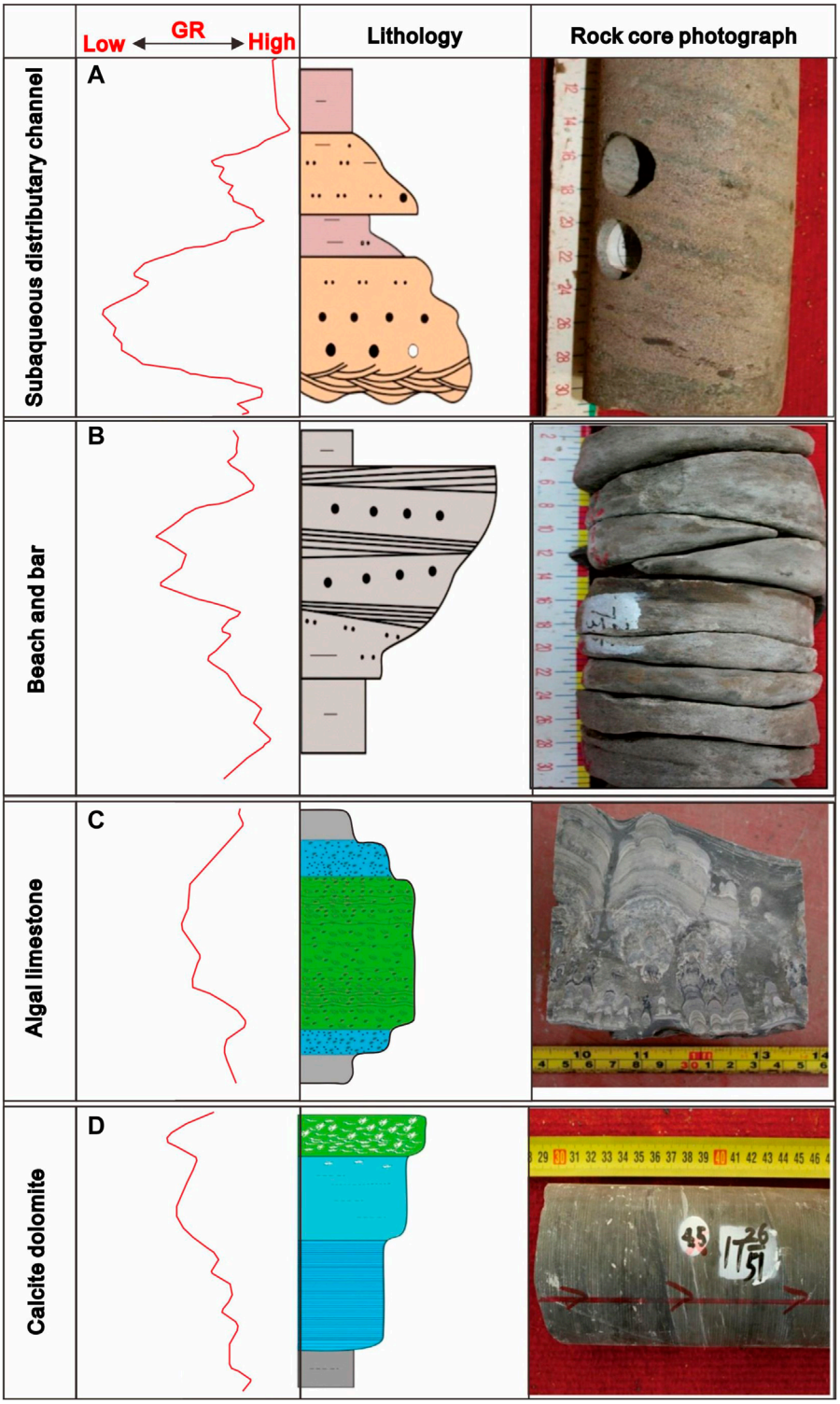

FIGURE 3
Typical log-sedimentary facies of outer belt **(A,B)** and middle belt **(C,D)**. **(A)** Delta front channel facies, the natural gamma is bell-shaped, and cross-bedding can be seen in the core. **(B)** Shallow lacustrine beach bar facies, natural gamma is funnel-shaped, and low-angle cross-bedding can be seen in the core. **(C)** Algae mound/algae mat facies, the natural curve is a low-amplitude box-shaped, and the lithology is mainly algal limestone. **(D)** The limy dolomite flat facies, the natural gamma is a low-amplitude toothed funnel shape, and the lithology is mainly limy dolomite.

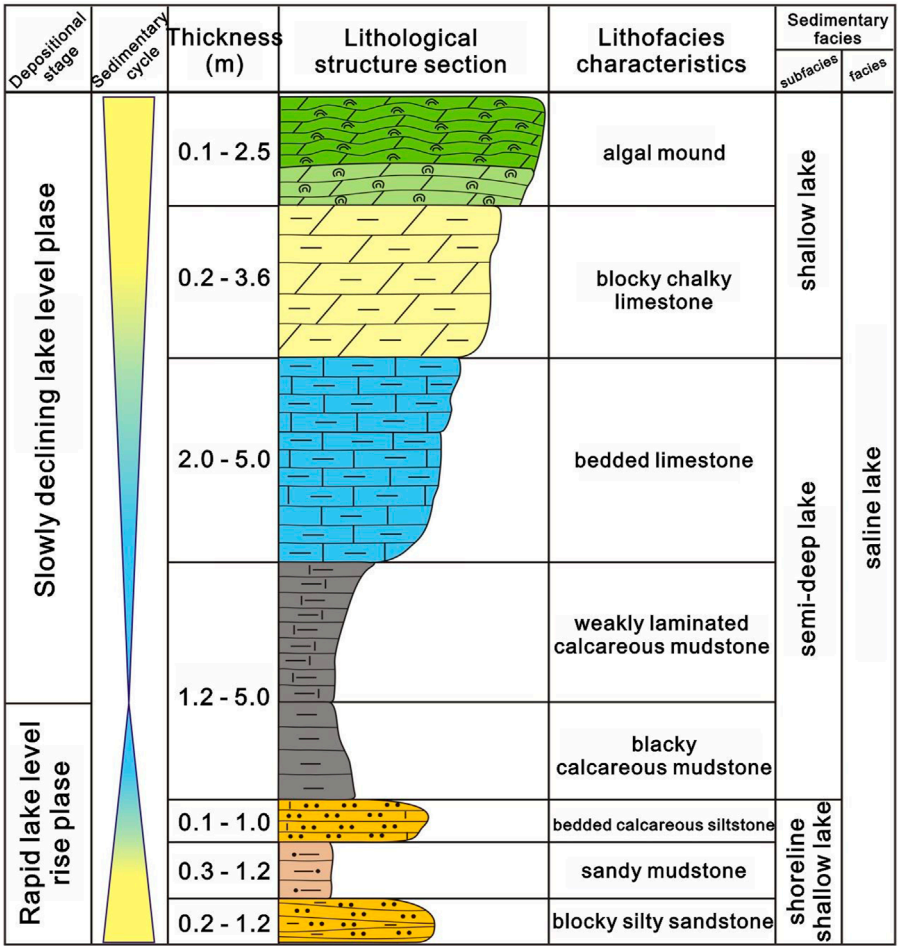

FIGURE 4
Sedimentary sequence diagram of the middle belt.

4.1.2 Lacustrine

In the Western Depression's near-shore shallow lacustrine environment, distinct zones such as beach and bar, algal limestone, and calcite dolomite are identified based on the proportion of terrigenous clastic rocks and carbonate minerals. The beach and bar zone is characterized by massive coarse-grained sandstone, exhibiting an inverse grain sequence and appears funnel-shaped on the gamma-ray (GR) log (Figure 3B). Algal limestone is marked by sedimentary structures associated with algal mats, alongside a high concentration of carbonate and clay minerals, presenting a smaller funnel-shaped GR log curve compared to the beach and bar, different shape features associated with biological processes can be seen in the core sequence (Figure 3C). Calcite dolomite, primarily formed under conditions of strong evaporation and located at the periphery of the saline lacustrine basin, features laminar structures and horizontal bedding (Figure 3D), with its GR log shape mirroring that of algal limestone. Beyond these zones, the mudflat area, characterized by fine sediments, predominantly consists of terrigenous clastic materials such as blocky silty sandstone, argillaceous siltstone, sandy mudstone, and bedded calcareous siltstone. Meanwhile, internal deposits comprise bedded limestone, blocky chalky limestone, and algal mounds, encapsulating a full lacustrine transgressive to regressive sequence (Figure 4).

In offshore semi-deep to deep lacustrine environments, black shale predominates within the transgressive sequences, where the content of clay minerals significantly exceeds that of carbonate minerals, featuring either weakly horizontal lamination or massive structures. During periods of intense evaporation in these semi-deep to deep lacustrine settings, a diverse assemblage of sediments forms, including heterogeneous sandstone, blocky muddy sandstone, argillaceous siltstone, and laminated calcareous shale from terrigenous clastic origins. Additionally, endogenous formations such as laminated dolomitic shale, lamellar mud-crystalline-pellet dolomite, and nodular gypsum-bearing dolomite contribute to a complete sedimentary cycle (Figure 5).

4.1.3 Cross-well sections

The northwest-southeast (NW-SE) profile indicates that terrigenous clasts predominantly originate from the mountain system along the northwest margin, diminishing in abundance from NW to SE (Figure 6; Rieser et al., 2005; Zhao et al., 2020). The lacustrine basin features two depocenters located between Xian

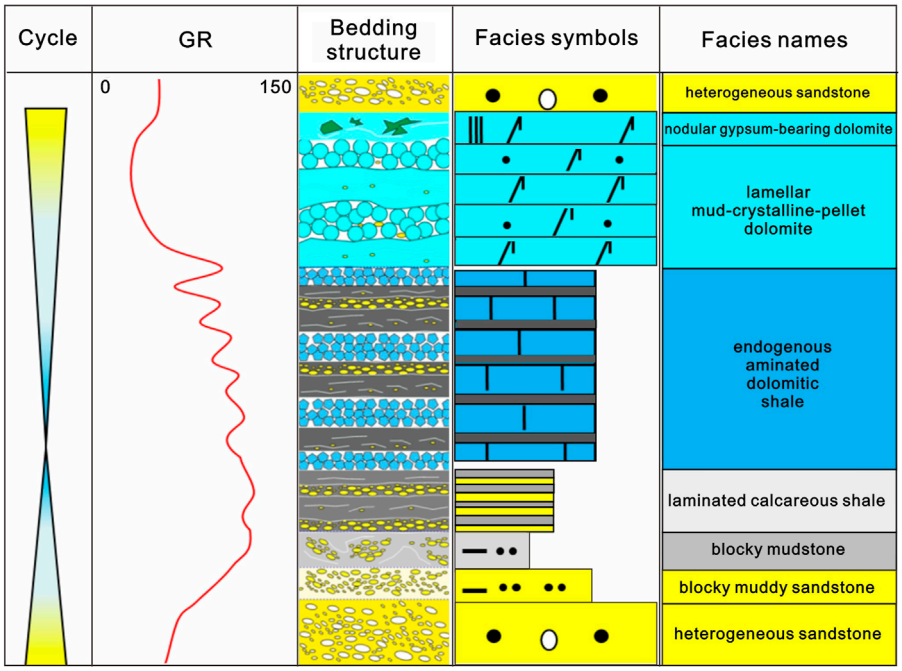

FIGURE 5
Sedimentary sequence diagram of the inner belt.

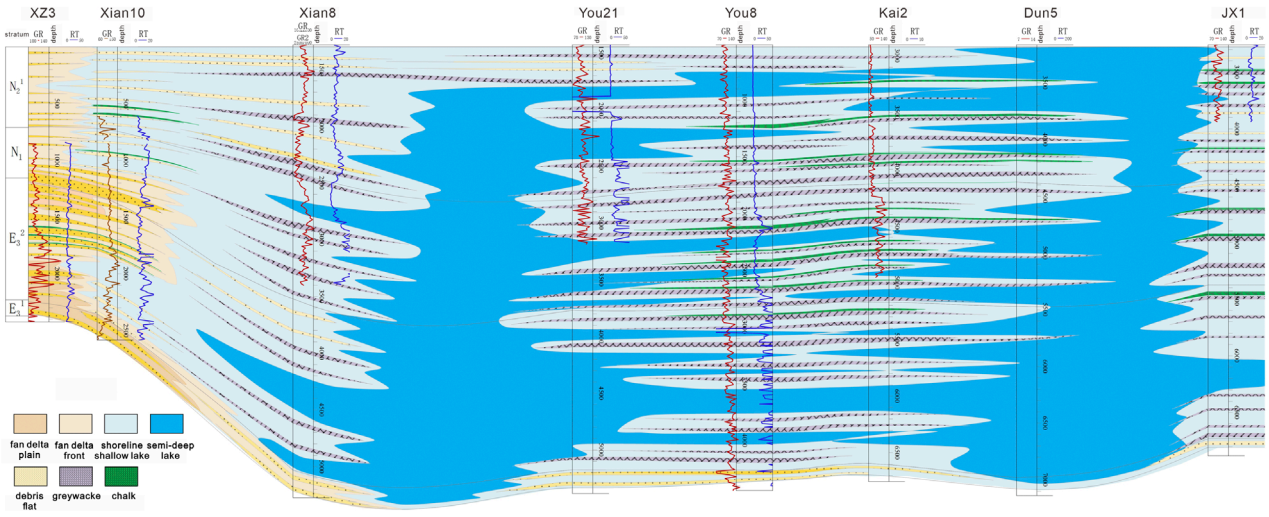

FIGURE 6
Sedimentary profile of NW-SE cross-well in the Western Depression.

8 and You 21, and Dun 5 and JX 1, respectively, with an uplift occurring in the region spanning You 21 to Dun 5 via You 8 and Kai 2. In the basin's center, the frequency of transitions between near-shore shallow lacustrine and offshore semi-deep to deep lacustrine facies associations results in aggradational sequences. In the southeast of this profile, the influx of terrigenous clastic material is minimal.

The southwest-northeast (SW-NE) profile reveals a progradational sedimentary sequence in the terrigenous coarse braided river delta, with the depocenter shifting from SX 58-Shi 60 to the Xian 8-Gou 5 area, influenced by the activity of the southwest Kunlun Mountain (Figure 7; Yuan et al., 2006). The section along SX 58-Chai 14 transitions from an offshore semi-deep to deep lacustrine at the base to a near-shore shallow lacustrine facies association at the surface. Both near the basin margin's near-shore shallow lacustrine and in the depocenter's offshore semi-deep to deep lacustrine facies associations exhibit aggradational sequences. Closer to the northeast provenance area, a fan delta forms, supported by the substantial input of terrigenous clastic material (Bush et al., 2016).

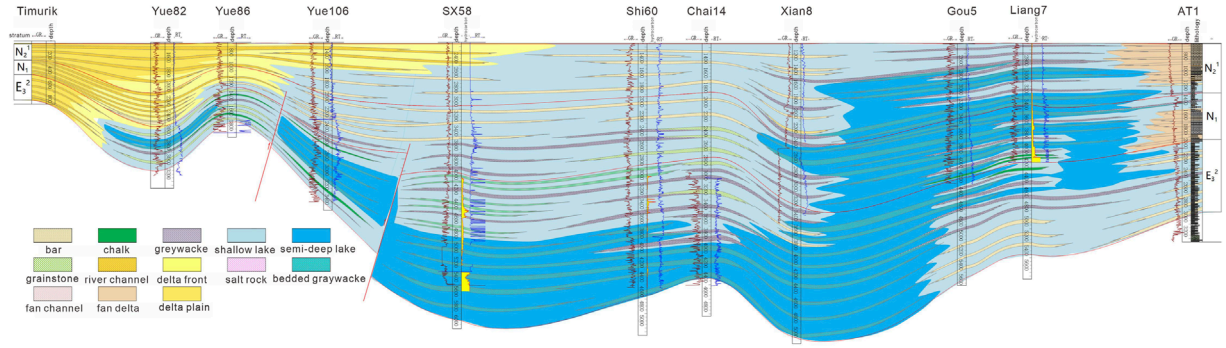

FIGURE 7
Sedimentary profile of SW-NE cross-well in the Western Depression.

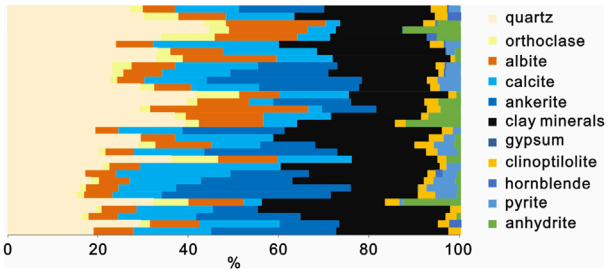

FIGURE 8
XRD diffraction pattern of a typical well in the outer belt (AT1).

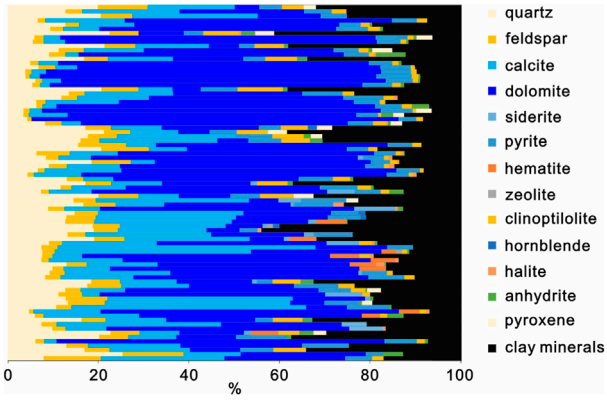

FIGURE 9
XRD diffraction pattern of a typical well in the middle belt (Qi 302).

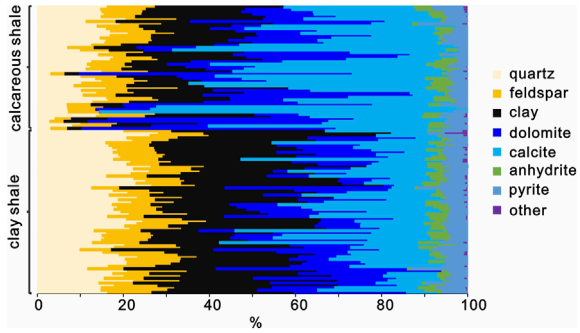

FIGURE 10
XRD diffraction pattern of a typical well in the inner belt (Chai 2-4).

4.2 Reservoir analysis

4.2.1 Petrology

Samples Qi 302 and Chai 2-4, representing near-shore shallow lacustrine and offshore semi-deep to deep lacustrine environments, respectively, were subjected to X-ray diffraction (XRD) analysis. The subaqueous distributary channel sandstone in the outer belt shows that the components are mainly quartz, clay minerals, and carbonate minerals, and the percentage of carbonate and clay minerals decreases with the increase of quartz (Figure 8). The analysis revealed that carbonate rocks in the near-shore shallow lacustrine environment exhibit the highest mineral content, predominantly comprising calcite, dolomite, and siderite, accounting for over 50% of the mineral composition. This is followed by felsic and clay minerals (Figure 9). Conversely, in the offshore semi-deep to deep lacustrine settings, the proportion of carbonate minerals significantly decreases, whereas clay minerals, anhydrite, and pyrite show a marked increase (Figure 10). Furthermore, the mineral composition within different lithofacies shales in the offshore semi-deep to deep lacustrine environment exhibits considerable variability. Endogenous calcareous shales are primarily composed of carbonate minerals, with a relatively low presence of felsic minerals. In contrast, felsic shales are characterized by a high concentration of felsic minerals and a reduced content of carbonate minerals.

4.2.2 Pore structure and type

Significant variations exist in the pore structure and types across reservoirs situated in different sedimentary facies. In the subaqueous distributary channels of the braided river delta front, sandstone cementation is notably weak, leading to the widespread development of intergranular pores with diameters

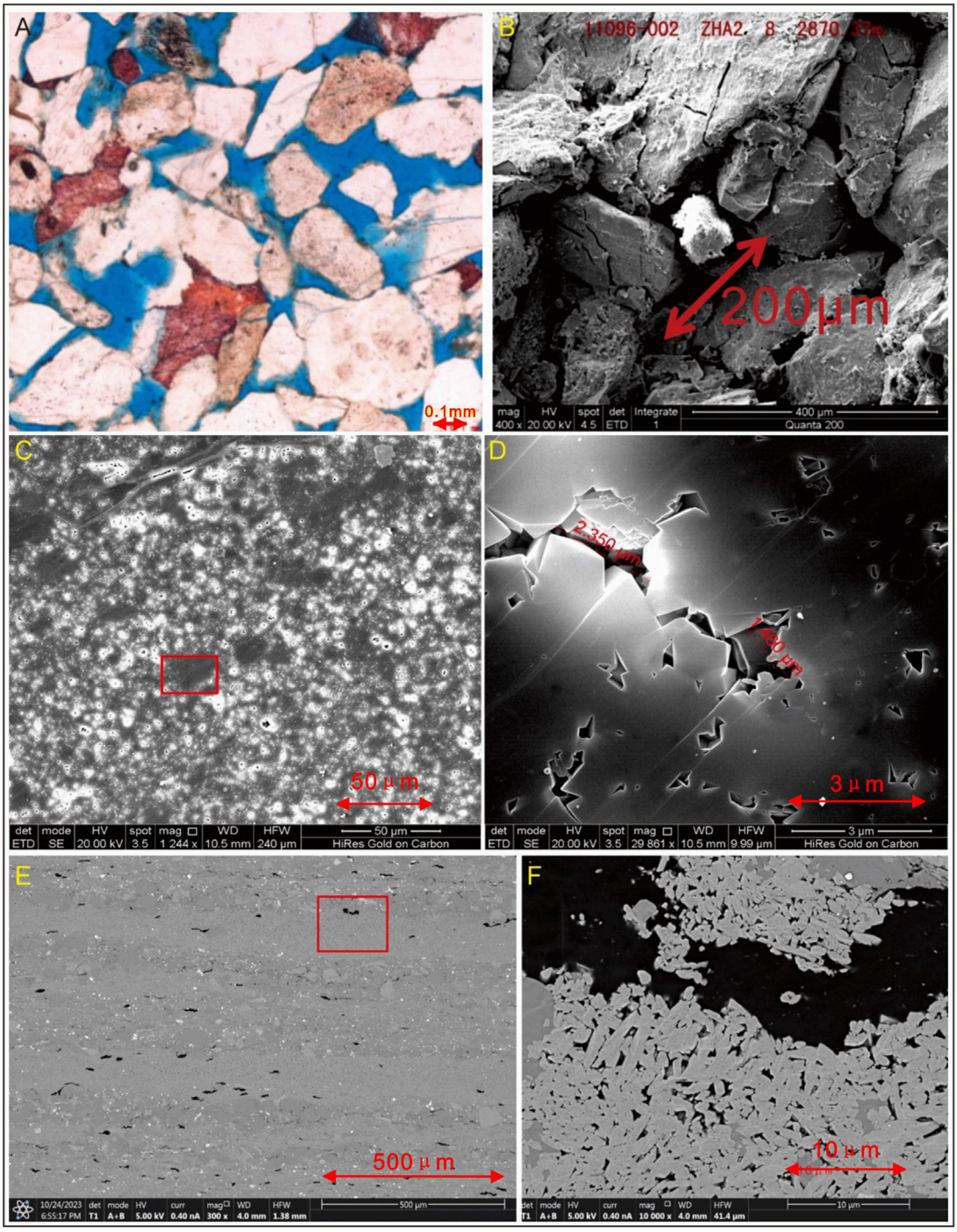

FIGURE 11
Typical reservoir characteristics of different ring-belt. **(A,B)**: Outer belt, delta front, subaqueous distributary channel sandstone. **(C,D)**: Middle belt, limy dolomite of the limy dolomite flat facies. **(E,F)**: Inner belt, laminated shale.

reaching up to 200 μm (Figures 11A, B). These pores typically exhibit lamellar and bundle throat types, demonstrating high connectivity. Conversely, the dominant pore types within near-shore shallow lacustrine limy dolomites are irregularly shaped dolomite intercrystalline pores, predominantly less than 3 μm in size (Figures 11C, D). Offshore semi-deep to deep lacustrine lamellar calcareous shales showcase irregular calcite-dissolved pores and intercrystalline pores, with sizes varying from 1 to 30 μm (Figures 11E, F). Notably, pores are absent in the argillaceous siltstone layers.

4.2.3 Porosity and permeability

The porosity and permeability of subaqueous distributary channel sandstones in the braided river delta front of the outer

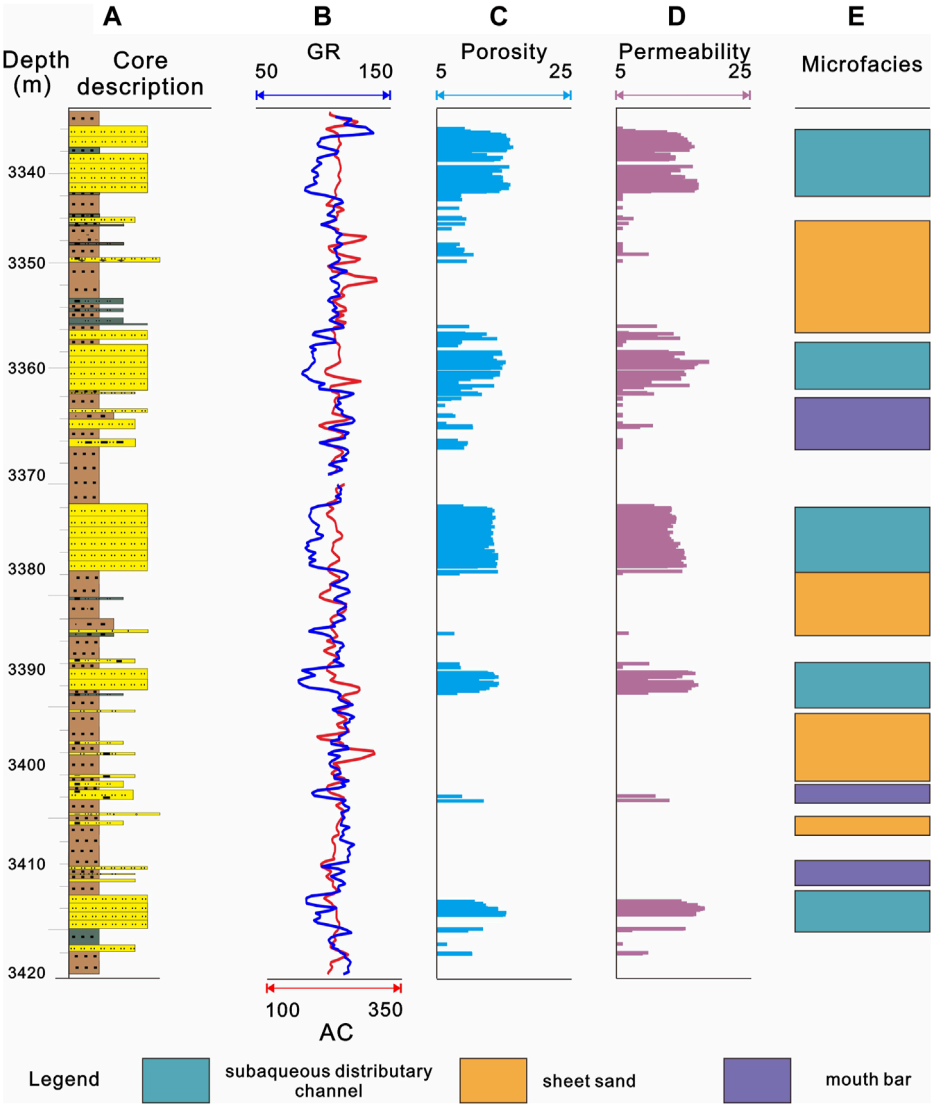

FIGURE 12
Comprehensive histogram of deposition and reservoirs of typical well in the outer belt. **(A)** Core description; **(B)** GR; **(C)** Porosity; **(D)** Permeability; **(E)** Microfacies.

belt exhibit favorable characteristics, with ranges of 5%–20% for porosity and 0.01–1,000 millidarcies (mD) for permeability, respectively. The average values for these properties are 15.8% and 547 mD, respectively, markedly surpassing those of sheet sand and mouth bar sandstones (Figure 12). Conversely, the porosity and permeability of near-shore shallow lacustrine limy dolomites of the middle belt display considerable heterogeneity, spanning 0%–12% and 0.01–10 mD, respectively (Figure 13). Notably, intervals of argillaceous limy dolomite and argillaceous limestone flat microfacies exhibit relatively higher porosity and permeability than beach and algal mat microfacies (Figure 13), alongside significant hydrocarbon indications. In the inner belt, the main distribution interval of porosity is 0%–5%, followed by 5%–7%, 7%–9%, and >9% and more than 90% of the samples have permeability less than 0.1 mD (Figure 14). In general, the reservoir property of outer belt is better than that of the middle belt, and the inner belt is worst.

5 Discussion

Detailed sedimentary facies and reservoir analyses are pivotal for predicting hydrocarbon-rich zones. A large number of provenance analysis studies have been carried out in the northwest margin of Qaidam Basin, which is located in the northern margin of the Tibet Plateau, and the provenance area has been confirmed, which provides convenience for the paleogeographic reconstruction in this paper (Rieser et al., 2005; Yuan et al., 2006; Zhao et al., 2020). Through comprehensive sedimentary facies analysis, the sedimentary infill processes, sediment dispersal patterns, and paleogeography of the Western Depression of the Qaidam Basin from the Paleogene to Neogene periods are elucidated (Figure 15). Sediment dispersal exhibits a ring-shaped distribution, originating from the outer belt's braided river and fan deltas, which are sourced from the Kunlun Mountains in the southwest and the Altun Mountains in the northwest, extending to the middle

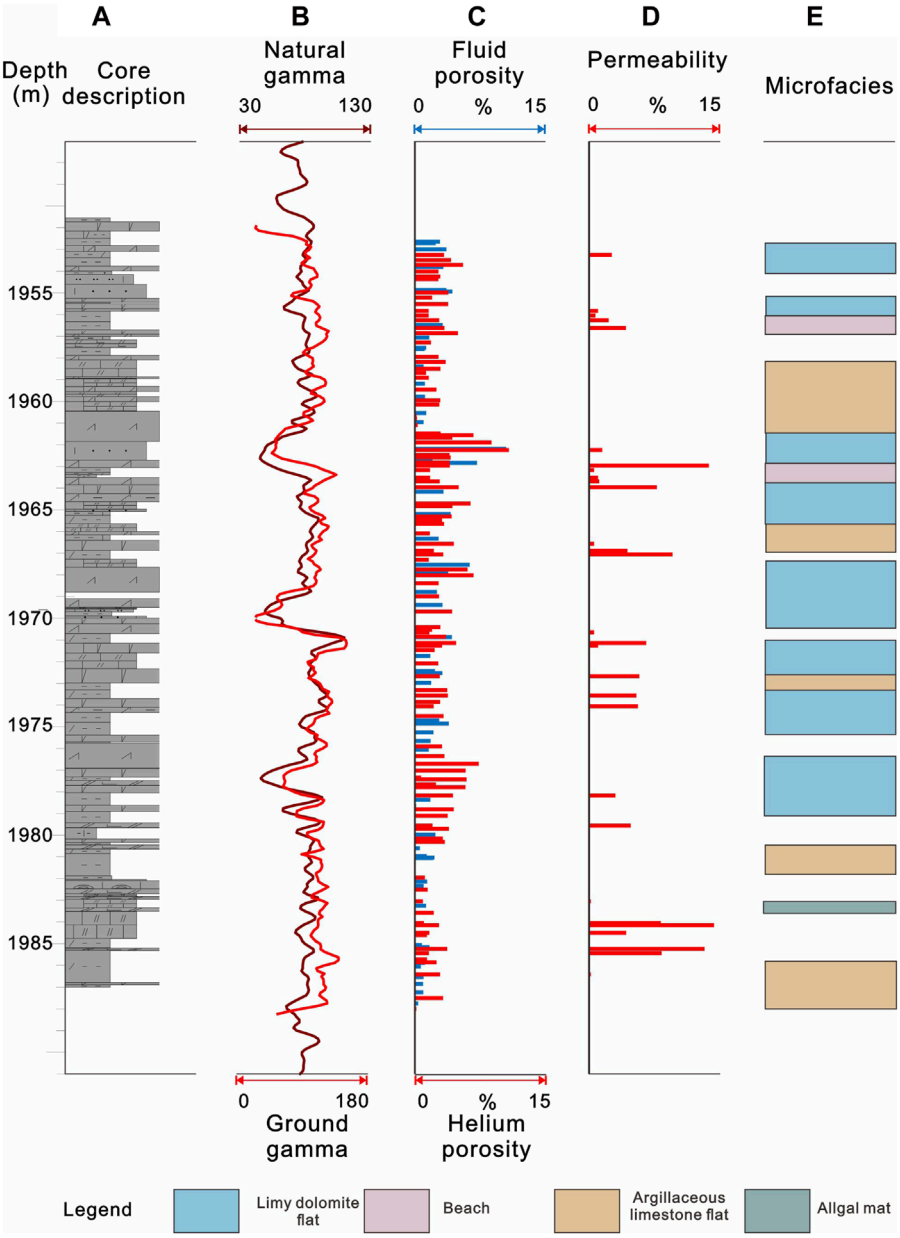

FIGURE 13
Comprehensive histogram of deposition and reservoirs of typical well in the middle belt. **(A)** Core description; **(B)** GR; **(C)** Porosity; **(D)** Permeability; **(E)** Microfacies.

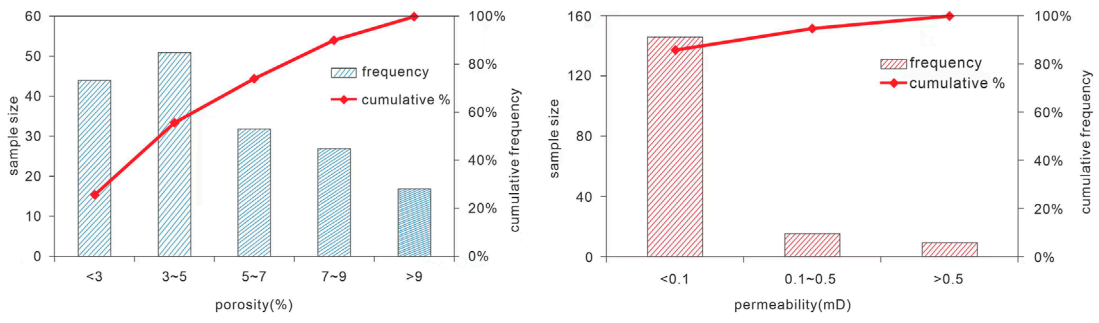

FIGURE 14
Comprehensive histogram of porosity and permeability of typical well in the inner belt.

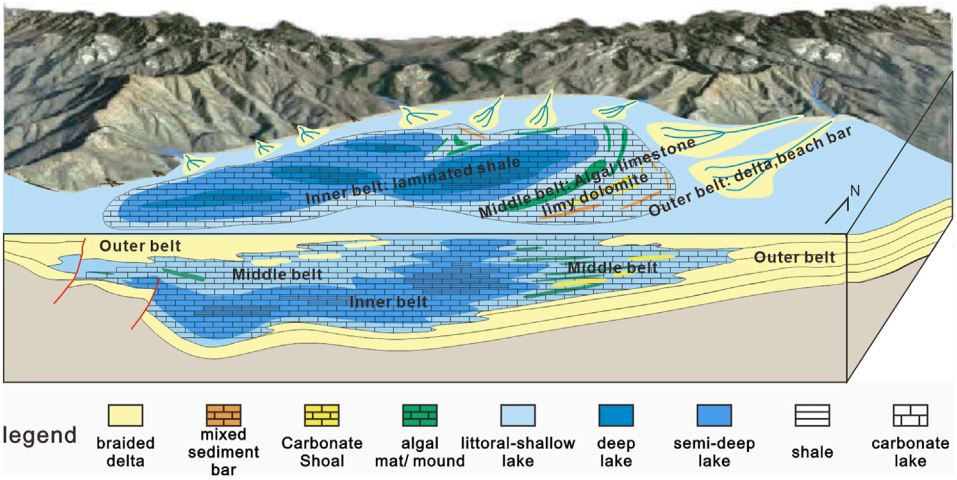

FIGURE 15
Ring-Zone depositional model diagram of the multi-type reservoir in Western Qaidam Basin (Modified from Li et al., 2023b).

belt characterized by beach and bars, algal mounds, and algal mats, and culminating in the inner belt with lamellar shales and bedded greywacke (Chen et al., 2015; Bao et al., 2017; He et al., 2021; Hou et al., 2022). Well and cross-section analyses reveal that the Kunlun Mountains' continuous uplift significantly influenced depositional patterns and the northwestern migration of the depocenter (Figure 7). The lake level fluctuation revealed by the sedimentary facies changes may be related to the tectonic and climatic controls (Rieser et al., 2009; Heermance et al., 2013; Herb et al., 2015). This regional interplay between source rocks and high-quality reservoirs outlines the spatial and temporal distribution relationships essential for exploration. The outer belt's coarse clastic reservoir, notable for its excellent porosity and permeability, emerges as the principal exploration target, achieving significant breakthroughs in structural trap exploration (Guo et al., 2017a; Liu et al., 2017). While porosity and permeability in the middle and inner belts do not match the outer belt's standards, their proximity to the source rock system presents a unique advantage. Despite heterogeneity, exploration efforts have identified the middle belt as having potential for lithologic trap exploration due to its relatively high porosity and permeability. In contrast, the inner belt shows promise for "source-reservoir matching" shale oil exploration (Zhang et al., 2018b; Li et al., 2022). Lacustrine level fluctuations facilitate lithologic trap formation, connecting source rocks in the inner belt to premium reservoirs of algal limestone and beach and bar facies in the middle belt (Figure 6). In the inner belt, carbonate rock layers and felsic silty shales with lamellar structures undergo dissolution by organic acids during hydrocarbon generation and expulsion, creating high-quality reservoirs and delineating key shale oil sweet spots (Figures 10, 11E).

Leveraging detailed sedimentological analysis and evaluating variations in petrology, pore structures, and the porosity and permeability across the outer, middle, and inner belts' reservoirs (Figures 8–14), this study elucidates the spatial and temporal distribution characteristics of high-quality reservoirs within the middle and inner belts (Figure 15). The high-quality reservoirs in the outer belt are mainly located in the subaqueous distributary channel sandstone of the braided river delta front near the Kunlun Mountains in the southwest margin of the Western Depression. The high-quality reservoirs in the middle belt are concentrated in algal mounds in the northeast margin of the Western Depression, with a continuous band shape. The high-quality reservoirs in the inner belt are distributed in the center of the lacustrine basin in a point shape because of their strong heterogeneity. This offers fresh insights for directing future oil and gas exploration endeavors in the Western Depression of the Qaidam Basin. It should be noted that the analysis of reservoir diagenesis and the origins of high-quality reservoirs has not been conducted in this study, representing a primary avenue for further research.

6 Conclusion

A detailed sedimentological analysis of the western depression of the Qaidam Basin reveals that it is composed of three sedimentary facies types: 1) Braided river and fan delta subaqueous distributary channels in the outer belt; 2) near-shore shallow lacustrine in the middle belt; 3) offshore semi-deep to deep lacustrine in the inner belt. The inner belt is the main area for shale oil exploration, including terrigenous sandstone, blocky muddy sandstone, argillaceous siltstone, laminated calcareous shale, endogenous laminated dolomitic shale, lamellar mud-crystalline-pellet dolomite, and nodular gypsum-bearing dolomite. Based on the spatial and temporal distribution characteristics of sedimentary facies and reservoirs, the ring-shaped exploration model is finally innovatively established.

Data availability statement

The raw data supporting the conclusion of this article will be made available by the authors, without undue reservation.

Author contributions

GL: Conceptualization, Investigation, Writing–original draft. JX: Conceptualization, Funding acquisition, Investigation, Writing–review and editing. KW: Data curation, Investigation, Visualization, Writing–review and editing. SW: Data curation, Investigation, Methodology, Writing–review and editing. BZ: Data curation, Methodology, Writing–review and editing. ZL: Data curation, Investigation, Visualization, Writing–review and editing. HX: Data curation, Investigation, Methodology, Writing–review and editing.

Funding

The author(s) declare that financial support was received for the research, authorship, and/or publication of this article. This research was jointly funded by the China National Petroleum Corporation major science and technology project "Continental Shale Oil Large-scale Reserves Increasing and Exploration and Development Techniques" (2023ZZ15).

Acknowledgments

We are grateful to Chenhao Wang and Pengcheng Zhang for their assistance.

Conflict of interest

Authors GL, JX, KW, BZ, and HX were employed by Qinghai Oilfield Company, PetroChina.

The remaining authors declare that the research was conducted in the absence of any commercial or financial relationships that could be construed as a potential conflict of interest.

Publisher's note

References

Angles, A., and Li, Y. L. (2017). The western Qaidam Basin as a potential Martian environmental analogue: an overview. *J. Geophys. Res. Planets* 122 (5), 856–888. doi:10.1002/2017JE005293

Arnaud, N., Tapponnier, P., Roger, F., Brunel, M., Scharer, U., Wen, C., et al. (2003). Evidence for mesozoic shear along the western Kunlun and altyn-tagh fault, northern tibet (China). *J. Geophys. Res. Solid Earth* 108, 2001JB000904. doi:10.1029/2001JB000904

Bailey, G. B., and Anderson, P. D. (1982). Applications of Landsat imagery to problems of petroleum exploration in Qaidam basin, China. *AAPG Bull.* 66 (9), 1348–1352. doi:10.1306/03B5A7A0-16D1-11D7-8645000102C1865D

Bao, J., Wang, Y. D., Song, C. H., Feng, Y., Hu, C. H., Zhong, S. R., et al. (2017). Cenozoic sediment flux in the Qaidam Basin, northern Tibetan Plateau, and implications with regional tectonics and climate. *Glob. Planet. Change* 155, 56–69. doi:10.1016/j.gloplacha.2017.03.006

Bush, M. A., Saylor, J. E., Horton, B. K., and Nie, J. S. (2016). Growth of the Qaidam Basin during Cenozoic exhumation in the northern Tibetan Plateau: inferences from depositional patterns and multiproxy detrital provenance signatures. *Lithosphere* 8, 58–82. doi:10.1130/L449.1

Chen, G. X., Zhao, F., Wang, J. G., Zhang, H. J., Yan, Y. Z., Wang, A. P., et al. (2015). Regionalized multiple-point stochastic geological modeling: a case from braided delta sedimentary reservoirs in Qaidam Basin, NW China. *Petroleum Explor. Dev.* 42 (5), 697–704. doi:10.1016/S1876-3804(15)30065-3

Cheng, F. A., Haproff, P., Wu, C., Neudorf, C., Chang, H., Li, X. Z., et al. (2021). Accommodation of India–Asia convergence via strike-slip faulting and block rotation in the Qilian Shan fold–thrust belt, northern margin of the Tibetan Plateau. *J. Geol. Soc.* 178 (3), jgs2020–207. doi:10.1144/jgs2020-207

Cowgill, E., Yin, A., Harrison, T. M., and Wang, X. F. (2003). Reconstruction of the Altyn Tagh fault based on U-Pb geochronology: role of back thrusts, mantle sutures, and heterogeneous crustal strength in forming the Tibetan Plateau. *J. Geophys. Res. Solid Earth* 108, 2002JB002080. doi:10.1029/2002JB002080

Dupont-Nivet, G., Butler, R. F., Yin, A., and Chen, X. H., (2002). Paleomagnetism indicates no Neogene rotation of the Qaidam Basin in northern tibet during indo-asian collision. *Geol.*, 30, 263–266.

Fang, X. M., Li, M. H., Wang, Z. R., Wang, J. Y., Li, J., Liu, X. M., et al. (2016). Oscillation of mineral compositions in core SG-1b, western Qaidam Basin, NE Tibetan Plateau. *Sci. Rep.* 6 (1), 32848. doi:10.1038/srep32848

Guo, J. J., Sun, G. Q., Long, G. H., Guan, B., Kang, J., Xia, W. M., et al. (2017a). Sedmentary diagenesis environment of the lower jurassic in lenghu V tectonic belt, northern Qaidam Basin. *Gas. Geosci.* 1672 - 1926, 12–1839. doi:10.11764/j.issn.1672-1926.2017.11.006

Guo, P., Liu, C. Y., Gibert, L., Huang, L., Zhang, D. W., and Dai, J. (2020). How to find high-quality petroleum source rocks in saline lacustrine basins: a case study from the Cenozoic Qaidam Basin, NW China. *Mar. petroleum Geol.* 111, 603–623. doi:10.1016/j.marpetgeo.2019.08.050

Guo, P., Liu, C. Y., Wang, L. Q., Zhang, G. Q., and Fu, X. G. (2019). Mineralogy and organic geochemistry of the terrestrial lacustrine pre-salt sediments in the Qaidam Basin: implications for good source rock development. *Mar. Petroleum Geol.* 107, 149–162. doi:10.1016/j.marpetgeo.2019.04.029

Guo, Z. Q., Ma, Y. S., Liu, W. H., Wang, L. Q., Tian, J. X., Zeng, X., et al. (2017b). Main factors controlling the formation of basement hydrocarbon reservoirs in the Qaidam Basin, western China. *J. Petroleum Sci. Eng.* 149, 244–255. doi:10.1016/j.petrol.2016.10.029

Hanson, A. D., Ritts, B. D., Zinniker, D., Moldowan, J. M., and Biffi, U. (2001). Upper Oligocene lacustrine source rocks and petroleum systems of the northern Qaidam basin, northwest China. *AAPG Bull.* 85 (4), 601–620. doi:10.1306/8626C95B-173B-11D7-8645000102C1865D

He, W. G., Barzgar, E., Feng, W. P., and Huang, L. (2021). Reservoirs patterns and key controlling factors of the Lenghu oil and gas field in the Qaidam Basin, northwestern China. *J. Earth Sci.* 32 (4), 1011–1021. doi:10.1007/s12583-020-1061-z

Heermance, R. V., Pullen, A., Kapp, P., Garzione, C. N., Bogue, S., Ding, L., et al. (2013). Climatic and tectonic controls on sedimentation and erosion during the Pliocene-Quaternary in the Qaidam Basin (China). *Geol. Soc. Am. Bull.* 125, 833–856. doi:10.1130/B30748.1

Herb, C., Koutsodendris, A., Zhang, W. L., Appel, E., Fang, X. M., Voigt, S., et al. (2015). Late Plio-Pleistocene humidity fluctuations in the western Qaidam Basin (NE Tibetan Plateau) revealed by an integrated magnetic–palynological record from lacustrine sediments. *Quat. Res.* 84 (3), 457–466. doi:10.1016/j.yqres.2015.09.009

Hou, H. H., Shao, L. Y., Li, Y. H., Liu, L., Liang, G. D., Zhang, W. L., et al. (2022). Effect of paleoclimate and paleoenvironment on organic matter accumulation in lacustrine shale: constraints from lithofacies and element geochemistry in the northern Qaidam Basin, NW China. *J. Petroleum Sci. Eng.* 208, 109350. doi:10.1016/j.petrol.2021.109350

Jian, X., Guan, P., Fu, L., Zhang, W., Shen, X. T., Fu, H. J., et al. (2023). Detrital zircon geochronology and provenance of cenozoic deposits in the qaidam basin, northern Tibetan plateau: an overview with new data, implications and perspectives. *Mar. Petroleum Geol.* 159, 106566. doi:10.1016/j.marpetgeo.2023.106566

Kane, O. I., Hu, M. Y., Cai, Q. S., Deng, Q. J., Yang, W. J., and Zuo, M. T. (2023). Sedimentary facies, lithofacies paleogeography, and an evaluation of the Ordovician sequences in the Sichuan Basin, southwest China. *Mar. Petroleum Geol.* 149, 106096. doi:10.1016/j.marpetgeo.2023.106096

Karplus, M. S., Zhao, W., Klemperer, S. L., Wu, Z., Mechie, J., Shi, D., et al. (2011). Injection of Tibetan crust beneath the south Qaidam Basin: evidence from INDEPTH IV wide-angle seismic data. *J. Geophys. Res. Solid Earth* 116 (B7), B07301. doi:10.1029/2010JB007911

Li, G. X., Wu, K. Y., Zhu, R. K., Zhang, Y. S., Wu, S. T., et al. (2023a). Enrichment model and high-efficiency production of thick plateau mountainous shale oil reservoir: a case study of the Yingxiongling shale oil reservoir in Qaidam Basin. *Acta Pet. Sin.* 44 (1), 144. doi:10.7623/syxb202301009

Li, G. X., Zhang, B., Wu, K. Y., Wu, S. T., Wang, X. M., Zhang, J., et al. (2023b). Low organic matter abundance and highly efficient hydrocarbon generation of saline source rock in the Qaidam Basin, NW China. *Petroleum Explor. Dev.* 50 (5), 1030–1044. doi:10.1016/S1876-3804(23)60447-1

Li, G. Y., Zhu, R. K., Zhang, Y. S., Chen, Y., Cui, J. W., Jiang, Y. H., et al. (2022). Geological characteristics, evaluation criteria and discovery significance of Paleogene Yingxiongling shale oil in Qaidam Basin, NW China. *Petroleum Explor. Dev.* 49 (1), 18–31. doi:10.1016/S1876-3804(22)60002-8

Li, W. (2004). The dynamics of the sedimentary system development and its implications for hydrocarbon accumulation in the Qaidam Basin. Dr. Dissertion.

Liu, Z. G., Zhang, Y. S., Song, G. Y., Li, S. M., Long, G. H., Zhao, J., et al. (2021). Mixed carbonate rocks lithofacies features and reservoirs controlling mechanisms in a saline lacustrine basin in Yingxi area, Qaidam Basin, NW China. *Petroleum Explor. Dev.* 48 (1), 80–94. doi:10.1016/S1876-3804(21)60006-X

Liu, Z. G., Zhu, C., Li, S. M., Xue, J. Q., Gong, Q. S., Wang, Y. Q., et al. (2017). Geological features and exploration fields of tight oil in the Cenozoic of western Qaidam Basin, NW China. *Petroleum Explor. Dev.* 44 (2), 217–225. doi:10.1016/S1876-3804(17)30024-1

Liu, C., He, H., Wang, Y. J., Hu, Y. F., Li, J. Y., Xie, L., et al. (2018). Sedimentary characteristics and sand-body superposition patterns of paleogene Braided River Delta in Q6 block of Kunbei Oilfield, Qaidam Basin. Journal of Xi'an Shiyou University. *Natur Sci.* 33.5, 25–33.

Lowenstein, T. K., Spencer, R. J., and Zhang, P. X. (1989). Origin of ancient potash evaporites: clues from the modern nonmarine Qaidam Basin of western China. *Science* 245 (4922), 1090–1092. doi:10.1126/science.245.4922.1090

Lu, H. J., Ye, J. C., Guo, L. C., Pan, J. W., Xiong, S. F., and Li, H. B. (2019). Towards a clarification of the provenance of Cenozoic sediments in the northern Qaidam Basin. *Lithosphere* 11 (2), 252–272. doi:10.1130/L1037.1

Metivier, F., Gaudemer, Y., Tapponnier, P., and Meyer, B. (1998). Northeastward growth of the Tibet plateau deduced from balanced reconstruction of two depositional areas: the Qaidam and Hexi Corridor basins, China. *Tectonics* 17, 823–842. doi:10.1029/98TC02764

Owen, L. A., Finkel, R. C., Ma, H. Z., and Barnard, P. L. (2006). Late Quaternary landscape evolution in the Kunlun Mountains and Qaidam Basin, Northern Tibet: a framework for examining the links between glaciation, lake level changes and alluvial fan formation. *Quat. Int.* 154–155, 73–86. doi:10.1016/j.quaint.2006.02.008

Phillips, F. M., Zreda, M. G., Ku, T. L., Luo, S., Huang, Q., Kubilk, P. W., et al. (1993) "230Th/234U and 36C1 dating of evaporite deposits from the western Qaidam Basin, China: implications for glacial-period dust export from Central Asia," *Geol. Soc. America Bull.*, 105, 1606–1616. doi:10.1130/0016-7606(1993)105<1606:TUACDO>2.3

Pullen, A., Kapp, P., McCallister, A. T., Chang, H., Gehrels, G. E., Garzione, C. N., et al. (2011). Qaidam Basin and northern Tibetan Plateau as dust sources for the Chinese Loess Plateau and paleoclimatic implications. *Geology* 39, 1031–1034. doi:10.1130/G32296.1

Rieser, A. B., Bojar, A.-V., Neubauer, F., Genser, J., Liu, Y. J., Ge, X.-H., et al. (2009). Monitoring Cenozoic climate evolution of northeastern Tibet: stable isotope constraints from the western Qaidam Basin, China. *Int. J. Earth Sci.* 98, 1063–1075. doi:10.1007/s00531-008-0304-5

Rieser, A. B., Liu, Y. J., Genser, J., Neubauer, F., Handler, R., Friedl, G., et al. (2006). 40Ar/39Ar ages of detrital white mica constrain the Cenozoic development of the intracontinental Qaidam Basin, China. *Geol. Soc. Am. Bull.* 118, 1522–1534. doi:10.1130/B25962.1

Rieser, A. B., Neubauer, F., Liu, Y. J., and Ge, X. H. (2005). Sandstone provenance of north-western sectors of the intracontinental Cenozoic Qaidam basin, western China: tectonic vs. climatic control. *Sediment. Geol.* 177, 1–18. doi:10.1016/j.sedgeo.2005.01.012

Rohrmann, A., Heermance, R., Kapp, P., and Cai, F. L. (2013). Wind as the primary driver of erosion in the Qaidam Basin, China. *Earth Planet. Sci. Lett.* 374, 1–10. doi:10.1016/j.epsl.2013.03.011

Schubel, K. A., and Lowenstein, T. K. (1997). Criteria for the recognition of shallow-perennial-saline-lake halites based on recent sediments from the Qaidam Basin, western China. *J. Sediment. Res.* 67 (1), 74–87. doi:10.1306/D42684FA-2B26-11D7-8648000102C1865D

Shi, Y. J., Yang, S. Y., Guo, J. J., Ma, X. M., Sun, X. J., Xu, L., et al. (2020). Deep hydrocarbon generation conditions and favorable zones in the Qaidam Basin. *J. China Univ. Min. Tech.* 51, 506–522.

Sun, G. Q., Wang, Y. T., Guo, J. J., Wang, M., Jiang, Y., and Pan, S. L. (2019). Clay minerals and element geochemistry of clastic reservoirs in the Xiaganchaigou Formation of the Lenghuqi area, northern Qaidam Basin, China. *Minerals* 9 (11), 678. doi:10.3390/min9110678

Sun, J. M., Zhang, Z. L., Cao, M. M., Windley, B. F., Tian, S. C., Sha, J. G., et al. (2020). Timing of seawater retreat from proto-Paratethys, sedimentary provenance, and tectonic rotations in the late Eocene-early Oligocene in the Tajik Basin, Central Asia. *Palaeogeogr. Palaeoclimatol. Palaeoecol.* 545, 109657. doi:10.1016/j.palaeo.2020.109657

Tan, X. F., Xia, M. Q., Zhang, Q. X., Wang, J., Huang, J. H., and Ran, T. (2016). Sedimentary characteristics of braided river delta of the lower member of the Lower Ganchaigou Formation in southwestern Qaidam Basin. *Oil Gas Geol.* 37 (3), 332–340. doi:10.11743/ogg20160305

Tang, W. B., Zhang, Y. Y., Pe-Piper, G., Piper, D. J. W., Guo, Z. J., and Li, W. (2021a). Permian to early Triassic tectono-sedimentary evolution of the Mahu sag, Junggar Basin, western China: sedimentological implications of the transition from rifting to tectonic inversion. *Mar. Petroleum Geol.* 123, 104730. doi:10.1016/j.marpetgeo.2020.104730

Tang, W. Q., Yi, F., Chen, X. D., Tang, H. L., Li, F. J., Xia, G. Q., et al. (2021b). Abrupt aridification in the upper eocene of the western Qaidam Basin, northeastern Tibetan Plateau. *Palaeogeogr. Palaeoclimatol. Palaeoecol.* 577, 110515. doi:10.1016/j.palaeo.2021.110515

Tapponnier, P., Zhiqin, X., Roger, F., Meyer, B., Arnaud, N., Wittlinger, G., et al. (2001). Oblique stepwise rise and growth of the tibet plateau. *Science* 294 (5547), 1671–1677. doi:10.1126/science.105978

Vengosh, A., Chivas, A. R., Starinsky, A., Kolodny, Y., Zhang, B. Z., and Zhang, P. X. (1995). Chemical and boron isotope compositions of non-marine brines from the Qaidam Basin, Qinghai, China. *Chem. Geol.* 120, 135–154. doi:10.1016/0009-2541(94)00118-R

Wang, J. G., Yang, S. Y., Li, X., Wu, Y. X., Gao, Y. F., Ma, X. M., et al. (2020). Characteristics and differential distribution of microbialites in saline lacustrines of the western Qaidam Basin. *J. China Univ. Min. Tech.* 2020, 1111–1127. doi:10.13247/j.cnki.jcumt.001180

Wang, Y. Q., Liu, Z. G., Song, G. Y., Zhu, C., Li, S. M., Wu, Y. X., et al. (2023). Development, sand control mechanism and hydrocarbon accumulation of beach-bar sandstone in a saline lacustrine basin: a case from the Neogene of southwestern Qaidam Basin, NW China. *Petroleum Explor. Dev.* 2023, 742–754. doi:10.11698/PED.20230057

Wei, H. F., Guan, P., Wang, H. F., and Wang, P. (2019). Research on petroleum geological conditions and exploration directions in mandong area of Qaidam Basin. *Geol. J. China Univ.* 25 (6), 943. doi:10.16108/j.issn1006-7493.2019054

Xia, G. Q., Wu, C. H., Li, G. J., Li, G. W., Yi, H. S., and Wagreich, M. (2021). Cenozoic growth of the eastern Kunlun range (northern Tibetan plateau): evidence from sedimentary records in the southwest Qaidam Basin. *Int. Geol. Rev.* 63 (6), 769–786. doi:10.1080/00206814.2020.1731717

Yang, L. J., Zhang, W. L., Fang, X. M., Cai, M. T., and Lu, Y. (2020). Aridification recorded by lithofacies and grain size in a continuous Pliocene-Quaternary lacustrine sediment record in the western Qaidam Basin, NE Tibetan Plateau. *Palaeogeogr. Palaeoclimatol. Palaeoecol.* 556, 109903. doi:10.1016/j.palaeo.2020.109903

Yuan, W. M., Dong, J. Q., Wang, S. C., and Carter, A. (2006). Apatite fission track evidence for Neogene uplift in the eastern Kunlun mountains, northern qinghai–tibet plateau, China. *J. Asian Earth Sci.* 27, 847–856. doi:10.1016/j.jseaes.2005.09.002

Zhang, T., Fang, X. M., Wang, Y. D., Song, C. H., Zhang, W. L., Yan, M. D., et al. (2018a). Late cenozoic tectonic activity of the altyn tagh range: constraints from sedimentary records from the western Qaidam Basin, NE Tibetan plateau. *Tectonophysics* 737, 40–56. doi:10.1016/j.tecto.2018.04.021

Zhang, W., Jian, X., Fu, L., Feng, F., and Guan, P. (2018b). Reservoir characterization and hydrocarbon accumulation in late Cenozoic lacustrine mixed carbonate-siliciclastic fine-grained deposits of the northwestern Qaidam basin, NW China. *Mar. Petroleum Geol.* 98, 675–686. doi:10.1016/j.marpetgeo.2018.09.008

Zhang, X., Liu, C. L., Guo, Z. Q., Gui, H. R., Tian, J. X., Wu, X. P., et al. (2020). Characteristics and influencing factors of unconventional hydrocarbon accumulation in saline lacustrine fine-grained sedimentary rocks in the northwestern Qaidam Basin. *Energy and fuels* 34 (3), 2726–2738. doi:10.1021/acs.energyfuels.9b03581

Zhao, D. S. (2006). Sedimentary systems of the lower section of the Xiaganchaigou Formation in the southwest Qaidam Basin and prediction of favorable sand bodies. Doctoral dissertation.

Zhao, J. F., Zeng, X., Tian, J. X., Hu, C., Wang, D., Yan, Z. D., et al. (2020). Provenance and paleogeography of the Jurassic Northwestern Qaidam Basin (NW China): evidence from sedimentary records and detrital zircon geochronology. *J. Asian Earth Sci.* 190, 104060. doi:10.1016/j.jseaes.2019.104060

Zheng, Y. S., Tang, W. Q., Yi, H. S., Pei, Z. W., Yang, M., Xing, H. T., et al. (2023). Oupling relationship between sedimentation of favorable intervals and lacustrine level change and its controlling factors in lacustrine tight reservoir: a case study of the Lower Shangganchaigou Formation in the Gasi area, western Qaidam Basin, China. *Sediment. Geol. Tethyan Geol.* 43 (3), 475–488. doi:10.19826/j.cnki.1009-3850.2022.04011

Zhu, C., Liu, Z. G., Song, G. Y., Long, G. H., Gong, Q. S., Zhao, J., et al. (2022). Sedimentary model,evolution and distribution of Paleogene lacustrine carbonate rocks in Yingxiongling structural belt. *Q. aidam Basin* 43 (11), 1558. doi:10.7623/syxb202211004